Computational Analysis and First Principle Study of Electrical and Optical Properties of Fe Doped SWBNNT and its Application

Abinash Thapa
Sikkim Manipal Institute of Technology
Bibek Chettri
Sikkim Manipal Institute of Technology
Arghyadeep Sarkar
McMaster University
Prashant Chandra Pradhan
Sikkim Manipal Institute of Technology
Bikash Sharma (ju.bikash@gmail.com)
Sikkim Manipal Institute of Technology https://orcid.org/0000-0003-2013-9686

Research Article

Keywords: Single-Walled Boron Nitride Nanotube, transition metal, Extended Huckel, Inductively Coupled Plasma

Posted Date: August 19th, 2021

DOI: https://doi.org/10.21203/rs.3.rs-599265/v1

Computational analysis and first principle study of electrical and optical properties of Fe doped SWBNNT and its application

Abinash Thapa[1], Bibek Chettri[2], Arghyadeep Sarkar[3], P C Pradhan[1] and Bikash Sharma[1*]
[1] Dept. of Electronics & Communication Engg., SMIT, SMU, Sikkim
[2] Dept. of Physics, SMIT, SMU, Sikkim
[3]Dept. of Electrical & Computer Engg., McMaster University

Corresponding Author: ju.bikash@gmail.com

Abstract-The electrical and optical properties of One Dimension-Single Walled Boron Nitride Nanotube (1D-SWBNNT) doped with transition metal Iron are studied using the Quantum ATK. Highest direct bandgap obtained for S1 as 5.3167eV and S3 as 3.5328eV depicted the possibility of its use as a dielectric in the memory device. SWBNNT showed a consistent bandgap for varying lengths of the NT. Bandgap tunability and a moderate increase in the number of states in Density of States (DOS) plots can be achieved by the inclusion of transition metal dopants in pristine SWBNNT. In Projected-DOS (PDOS) plots we observed N and Fe atoms as the majority contributor of electronic states in the valence band and Fe atom as the main contributor in the conduction band. The inclusion of Fe dopant leads to an increase in the wavelength and optical gap. High optical conductivity for S2, S3, and S4 depicts its use as composites in photoconductive devices. The incorporation of Fe dopant led to a rise in susceptibility (χ) where S1 and S2-S4 showed a weak diamagnetic and strong paramagnetic property. BNNTs technologies are still growing, there is a need for further development bringing out its vast applications in the future.

Keywords- *Single-Walled Boron Nitride Nanotube, transition metal, Extended Huckel, Inductively Coupled Plasma*

I. INTRODUCTION

Boron Nitride Nanotubes (BNNTs) have been a revolutionary new Low-Dimensional (LD) material that is being extensively studied [1, 2]. BNNTs have a constant bandgap that does not depend on the radius and helicity as compared to CNTs [3] and have better oxidation and corrosion resistance at high temperatures [4, 5]. Thus, it is highly considered as a possible alternative to CNTs [6]. It is lightweight and the strongest nanomaterial with Young's Modulus of 1.3TPa and tensile strength of 33Gpa [7]. Applications of BNNTs are as an electrical insulator, piezoelectric/ceramic composites, biomedical devices, fire retardant cabling, polymer composites, and radiation shielding [8-11].

The literature survey indicated a research gap in studying the interaction of SWBNNT with strong ferromagnetic transition metal i.e., Fe. BNNT showed a higher vulnerability to doping [12-15] and functionalization [16, 17]. This paper provides a detailed study of electrical properties like effective mass, Density of States (DOS), bandstructure, and Projected-DOS (PDOS). And optical properties such as absorption (α_a), dielectric constant (ε), extinction (k) and refractive index (η), optical conductivity (σ), reflectivity (r), and susceptibility (χ). Understanding the electrical and optical properties of nanotubes helps in validating its application in nanoelectronics and optoelectronic device [18, 19].

II. METHODOLOGY

The atomistic calculation was performed using Extended Huckel (EH) based on the tight-binding (TB) model [20]. SWBNNT structure is constructed with $1\times1\times4$ repetitions and chirality (8,0), the diameter of 6.27Å, and thickness of 13.17Å as shown in Fig.1. Four samples considered for our study are **Sample1 (S1)**: pristine (8,0) SWBNNTs, **Sample2 (S2)**: substitution of B by Fe atom, **Sample3 (S3)**: substitution of N by Fe atom, and **Sample4 (S4)**: substitution of B-N by two Fe atoms (2Fe). Table I shows the details of doping concentration and fermi energy of SWBNNT samples.

Density mesh cut-off of 150Ry, Fermi-Dirac occupation, and boarding temperature of 1200K for all the samples [21]. The Brillion zone was sampled at $1\times1\times50$ *k*-points using Monkhorst-Pack grid Scheme.

Pulay mixer algorithm with the tolerance of 0.0002Ry, maximum steps of 100, and damping factor of 0.1 was used for controlling self-consistent iteration [21]. The geometric optimization was carried out for SWBNNT samples using Tersoff Potential with force tolerance of 0.05eV/Å and maximum steps of 10 [21]. Fe as dopant was embedded at different sites in S2, S3, and S4 samples shown in Fig.1(b)-(d). The resultant bond length of 1.41Å and bond angle of 120.16º are obtained for S2 and S3 having Fe as dopant substitution with Fe-N and Fe-B. Similarly, for S4 we obtained a bond length of 1.42Å and a bond angle of 120º.

Optical properties were investigated at optical spectrum energy range from 0 to 5eV with 101 sample points [22]. The Low Range Energy (LRE) varies from 0 to 2.5eV and High Range Energy (HRE) varies from 2.5 to 5eV [22].

Table I: Doping concentration and Fermi Energy of SWBNNT samples

Sample	Doping Concentration (%)	Fermi Energy E_f (eV)
1	Undoped	-9.492
2	1.042	-10.13
3	1.042	-11.77
4	2.083	-10.20

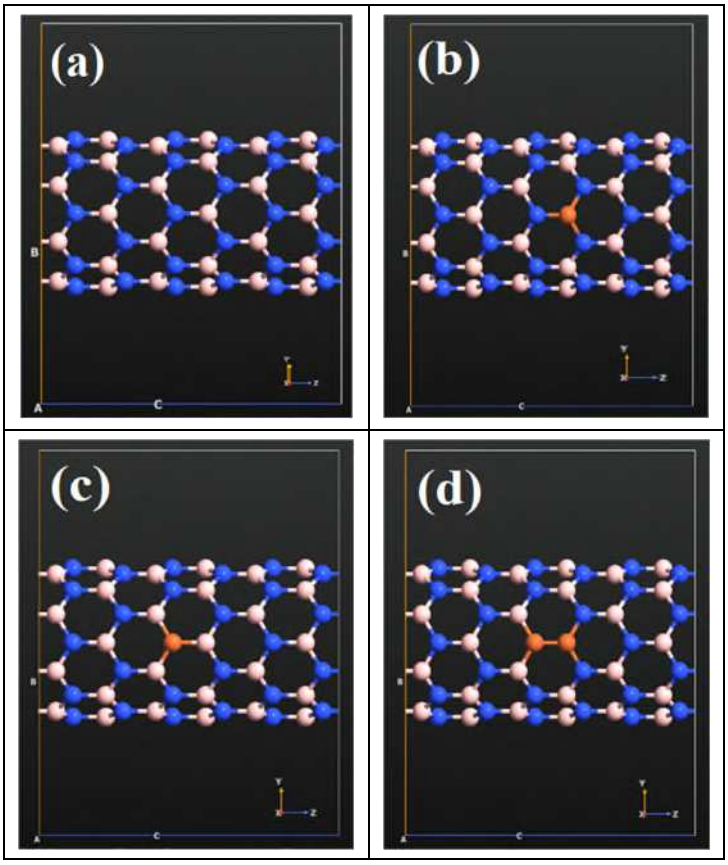

Fig.1 Geometric structure of SWBNNT (a) S1, (b) S2, (c) S3, and (d) S4

III. RESULTS & DISCUSSION

A. Electrical Properties of BNNT

BNNT predicted a wide bandgap of 5eV [3, 23, 24] which can be tuned by interaction with metal atoms [25]. Wide bandgap nanomaterials find good applications as composites in nanodevice, biodegradable polymers, and nanomedicines [26].

Effective Mass

The effective mass, band index, and energy calculation for SWBNNT samples are shown in Table II. The effective mass of pristine SWBNNT is 4.09E9. Further addition of heavy transition metal i.e., Fe to pure SWBNNT led to an increase in the effective mass of the sample. The effective mass of S2, S3, and S4 increases to 130.9E9, 43.6E9, and 523.6E9, respectively. It states that the effective mass of LD-material depends on the concentration of dopant added. An increase in effective mass causes the crossing of bands at the Fermi energy (E_f) in bandstructure plots.

Table II: Effective Mass, band index, and energy of four sample SWBNNT

Sample	Band index	Energy (eV)	$m \times (m_e)$
1	191	-2.701	4.09E9
2	193	-0.153	130.9E9
3	192	-0.171	43.6E9
4	195	-0.074	523.6E9

Bandstructure and DOS

The bandgap is an important parameter that restrains material application and nanoelectronics device performance such as conductivity, sensitivity, and optical sensing range [27-30]. The direct bandgap of 5.3167eV and 3.5328eV at Γ point was observed for S1 and S2 samples. Quantum confinement leads to a higher bandgap in S1 and S2 with negligible temperature effects [31], provides its usefulness in high-power electronic device applications and as dielectric composites in Magnetic Tunnel Junction (MTJ) device [32]. A minimum direct bandgap of 0.1448eV and 1.7113eV at Γ point was observed for S2 and S4 depicting semiconductor/metallic characteristics respectively. The addition of Fe dopants has significantly reduced the direct bandgap and exhibits semiconducting properties for S2, S3, and S4 samples [33-37]. Table III shows the SWBNNT samples bandgap and its applicability.

Another important observation was made, when the length of pristine SWBNNTs was increased (at 11.37Å, 24.15Å, and 49.73Å) a constant bandgap was obtained. Whereas in the case of CNT/SiCNT, the bandgap increases with an increase in the length of nanotubes. Thus defines the bandgap consistency of SWBNNT which does not depend on its radius and length [38].

Table III: SWBNTT samples bandgap, and their applicability

Sample	Bandgap (eV)	VB edge (eV)	CB edge (eV)	Applicability
1	5.3167	-2.7014	2.6153	Insulator
2	1.7113	-0.0791	1.6322	Semiconductor
3	3.5328	-0.1145	3.1341	Insulator
4	0.1448	-0.0709	-0.0730	Semiconductor/metallic

From DOS plots we observed that the S1, S2, S3, and S4 samples have the highest peak at -4eV, -3.5eV, -2.5eV, and -3.2eV in Valence Band (VB), respectively as shown in Fig.2. The maximum number of states were observed in S2, S3 and S4 contributed by p-orbital as shown in Fig.2(c)-(d), depicting applications in optoelectronic devices [39-41]. Hence, the addition of Fe dopants leads to an increase

in the number of peaks in DOS plots as shown in Fig.2(a)-(d), illustrate the application of SWBNNT as dielectrics in MTJ memory device with a high number of DOS states [22].

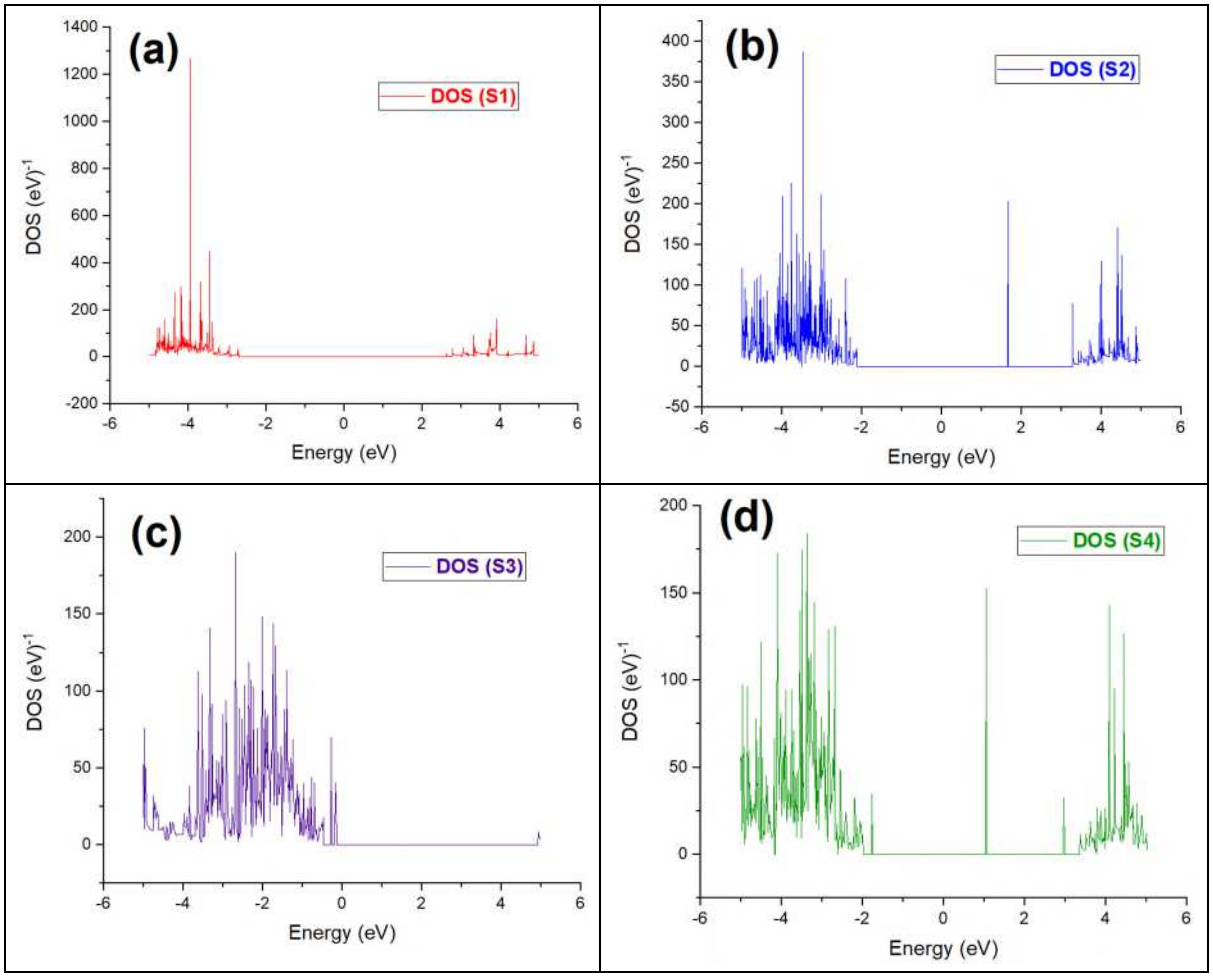

Fig.2 Density of States (DOS) vs Energy (eV) of (a) S1 (red), (b) S2 (blue), (c) S3 (purple), and (d) S4 (green)

Projected-DOS (PDOS)

PDOS plots for SWBNNT samples are shown in Fig.3(a)-(d). PDOS plot for S1 defines the even contribution of B and N shells in VB and CB as shown in Fig.3(a). S2, S3, and S4 predict the majority contribution of electronic state by Fe atom of L2 shell, N atoms of the L1 shell, and N atoms of L1 shell in the VB as shown in Fig.3(b)-(d). The cause of uneven charge distribution is due to unsymmetric Fe doped observed in PDOS plots for S2 and S3, resulting in a negligible electronic state in CB. Except for S4 having symmetry Fe doped leads to contributed of electronic state by Fe atoms of L2 shell in CB [42]. Uneven charge distribution between Fe atoms observed in PDOS plots is defined due to the lower electronegativity of Fe atoms compared to B (~2.04) and N (~3.04) atoms [22]. As more electrons are attracted by nitrogen atoms because of higher electronegativity [22].

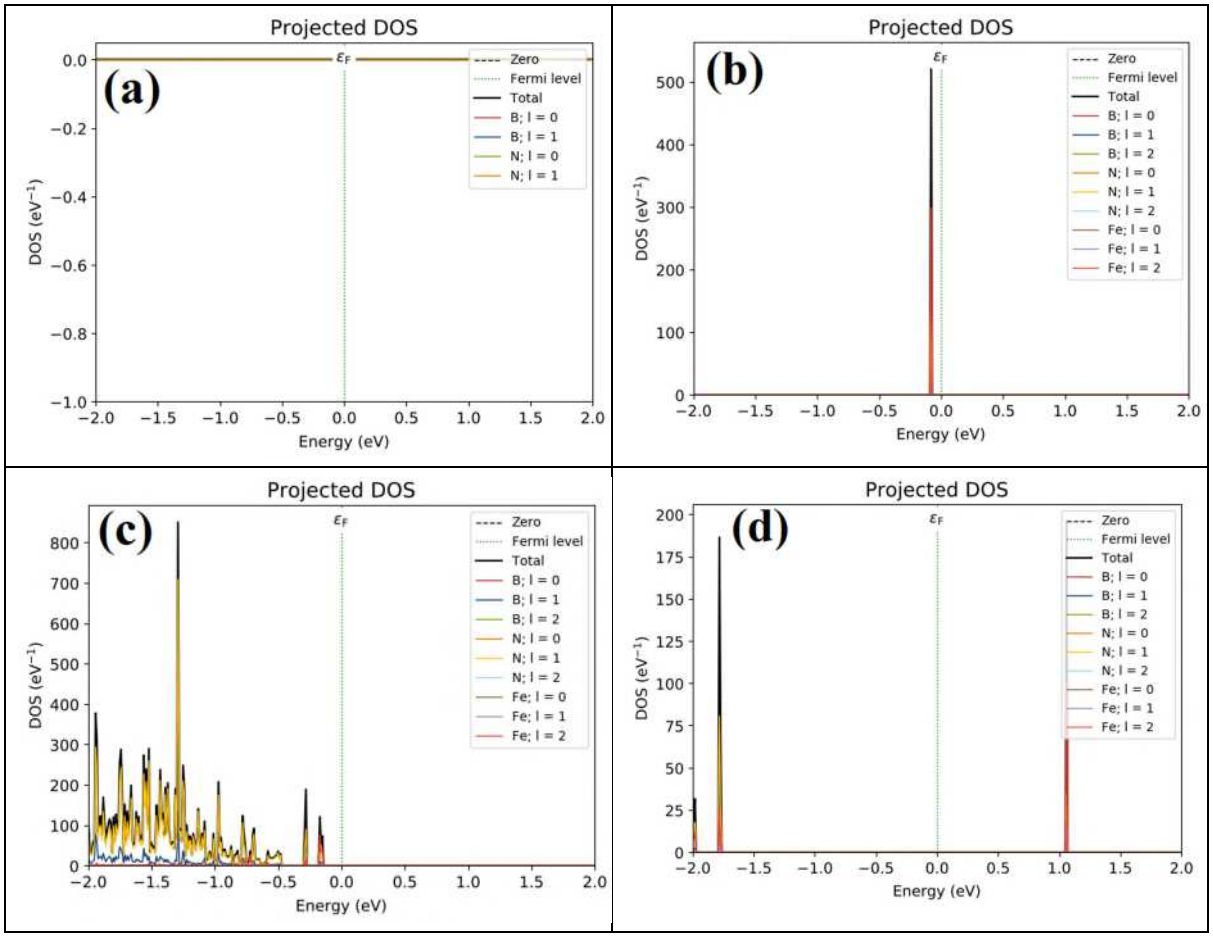

Fig.3 PDOS vs Energy (eV) plots of (a) S1, (b) S2, (c) S3, and (d) S4

B. Optical properties of BNNT

Investigating the optical properties of nanotubes is a new domain of interest in nanoscience [43]. The SWBNNT axis is set along the z-direction with Low Range Energy (LRE) range from 0-2.5eV and High Range Energy (HRE) range from 2.5-5eV for studying the optical properties [22]. This paper provides the study of optical properties of Fe doped SWBNNTs, as the same has not been explored much.

Optical Absorption (α_a)

Absorption predicts the photoluminescence property of optical materials [44, 45]. Optical absorption coefficient ($\alpha(\omega)$) is given as,

$$\alpha(\omega) = 2\omega\sqrt{\frac{1}{2}\left[-\varepsilon(\omega) + \sqrt{\varepsilon_1(\omega)^2 + \varepsilon_2(\omega)^2}\right]} \qquad (1)$$

Where, ω is the unit of energy, $\varepsilon_1(\omega)$ and $\varepsilon_2(\omega)$ are real and imaginary dielectric function.

Optical absorption vs energy(eV): Observing α_a plot for S1, the LRE to HRE indicating the no peak contribution along xx/yy/zz direction determines its high reflectivity and insulating property. The highest peak was observed along xx direction in LRE for S2 as shown in Fig.4(a). Absorption peak in LRE appears due to sum over allowed band transition from occupied valance states to empty conduction state [22]. For S3 α_a plot showed the highest peak along xx/yy/zz at HRE because of allowed band transition from empty conduction states to occupied valance states [22]. The LRE to HRE indicates the highest peak along xx/yy direction for S4 as shown in Fig.4(a) & (b). Two major peaks denote sub-band transition caused by first and second peaks for 2Fe doped S4.

A constant optical gap of SWBNNT (S2 and S3) has applications in nano-optoelectronic devices for the absorption of harmful ultraviolet light [22]. Multiple peaks were observed for S4 shown in Fig.4 due to the addition of 2Fe dopant, distorting its previous absorption parameters. The dual highest peak was observed at 1.2eV for S4. The highest optical gap peak for S3 of 5.71E-8cm, S4 of 1E-5cm, and S2 of 1.11E-5cm signify monochromatic nature and larger absorption intensity. Hence, finding applications in photodetector devices for wavelength detection [22].

Optical absorption vs wavelength(nm): BNNTs are also considered as a promising electron emission material due to their negative electron affinity (NEA) [22]. No visible light spectrum was emitted while observing the absorption vs wavelength (λ) plot for S1. λ of 700nm (red light), 300nm (UV light), and 5000nm (Infrared light) were observed for S2, S3, and S4 and predicting its use as composites in LEDs, medical devices and sensor applications [44].

Comparison between absorption and luminescence measurement helps to reinterpret band and correlate absorption and emission [22]. Table IV shows the calculated Absorption peak, Energy, and Wavelength of SWBNNT samples. The addition of Fe dopant leads to an increase in the wavelength and optical gap.

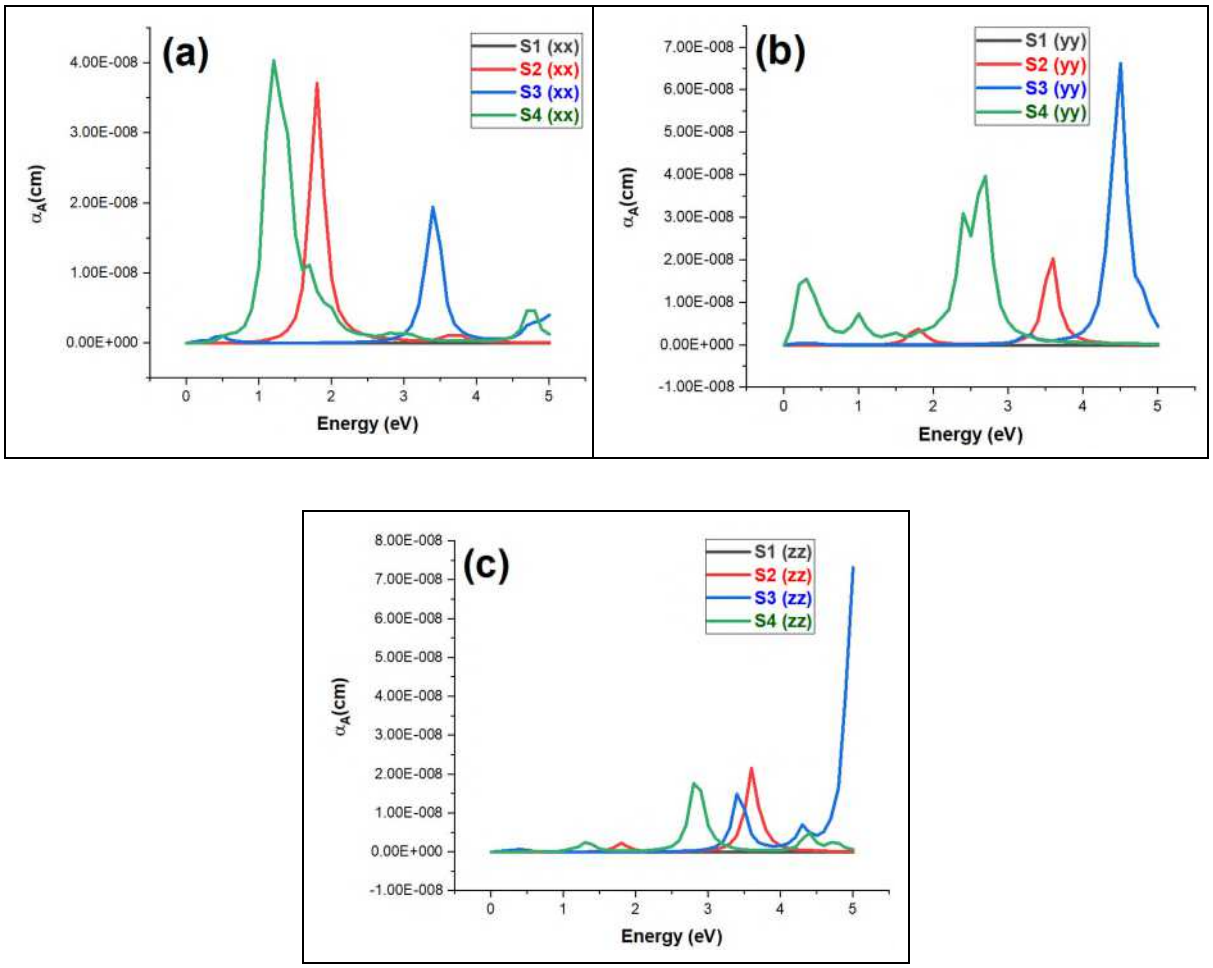

Fig.4 Absorption Vs Energy (eV) of S1, S2, S3, and S4 along (a) xx, (b) yy, and (c) zz direction

Table IV: Calculation of Absorption, Energy, and Wavelength of SWBNNT samples

Sample SWBNNT	1st peak Absorption (cm)	Energy (eV)	Wavelength (nm)	2nd peak Absorption (cm)	Energy (eV)	Wavelength (nm)
1	Nil	Nil	Nil	Nil	Nil	Nil
2	1.11E-5	2	700 (red)	1.82E-5	3.6	300 (near ultraviolet)
3	5.71E-6	5	300 (near ultraviolet)	1E-5	4.5	2700 (Infrared)
4	1E-5	1.2	5000 (Infrared)	1.82E-5	3	450 (Blue)

Dielectric constant (ε)

Dielectric function (ε) consists of real ($\varepsilon_1(\omega)$) and imaginary part ($\varepsilon_2(\omega)$) [44] given as,

$$\varepsilon(\omega) = \varepsilon_1(\omega) + i\varepsilon_2(\omega) \qquad (2)$$

Where $\varepsilon_1(\omega)$ and $\varepsilon_2(\omega)$ are the incoming light frequency of real and imaginary part of the dielectric function, respectively. The imaginary part of the dielectric constant illustrates the optical gap of SWBNNTs [22]. The peaks in the imaginary part ε_i denote direct interband transitions between the Van-Hove (VHs). Distinctly two VHs transition of E_1 and E_2 was observed for S2, S3, and S4 along zz direction as shown in Fig.5(a)-(c). No peaks were observed in real and imaginary dielectric constant plots determining the low dielectric constant (Ɛ~1) value of pristine SWBNNT (S1). Table V shows the real dielectric constant value at 0eV for S1, S2, S3, and S4 along xx, yy, and zz direction.

Table V: Real dielectric constant value at 0eV for S1, S2, S3, and S4 along xx, yy, and zz direction

Samples	S1 at 0eV	S2 at 0eV	S3 at 0eV	S4 at 0eV
Re[Ɛ] along xx direction	1	1.12368	1.20838	1.51868
Re[Ɛ] along yy direction	1	1.03508	1.23824	8.86546
Re[Ɛ] along zz direction	1	1.02256	1.23392	1.05616

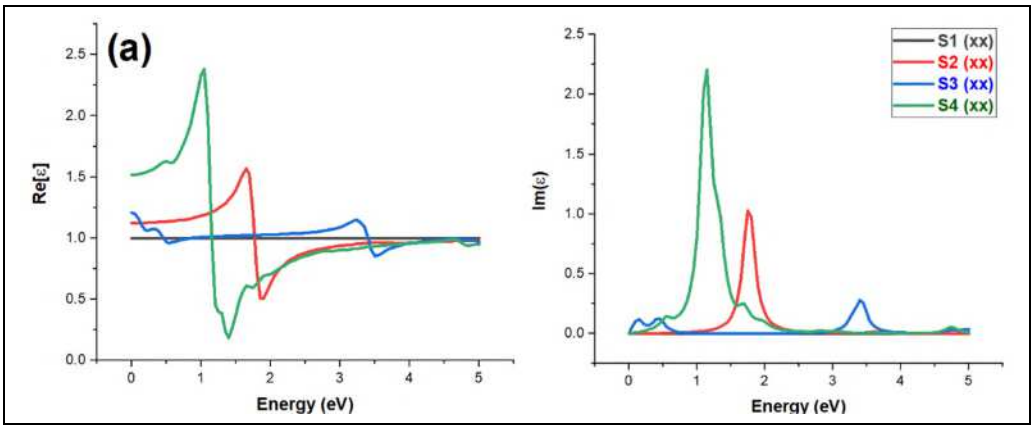

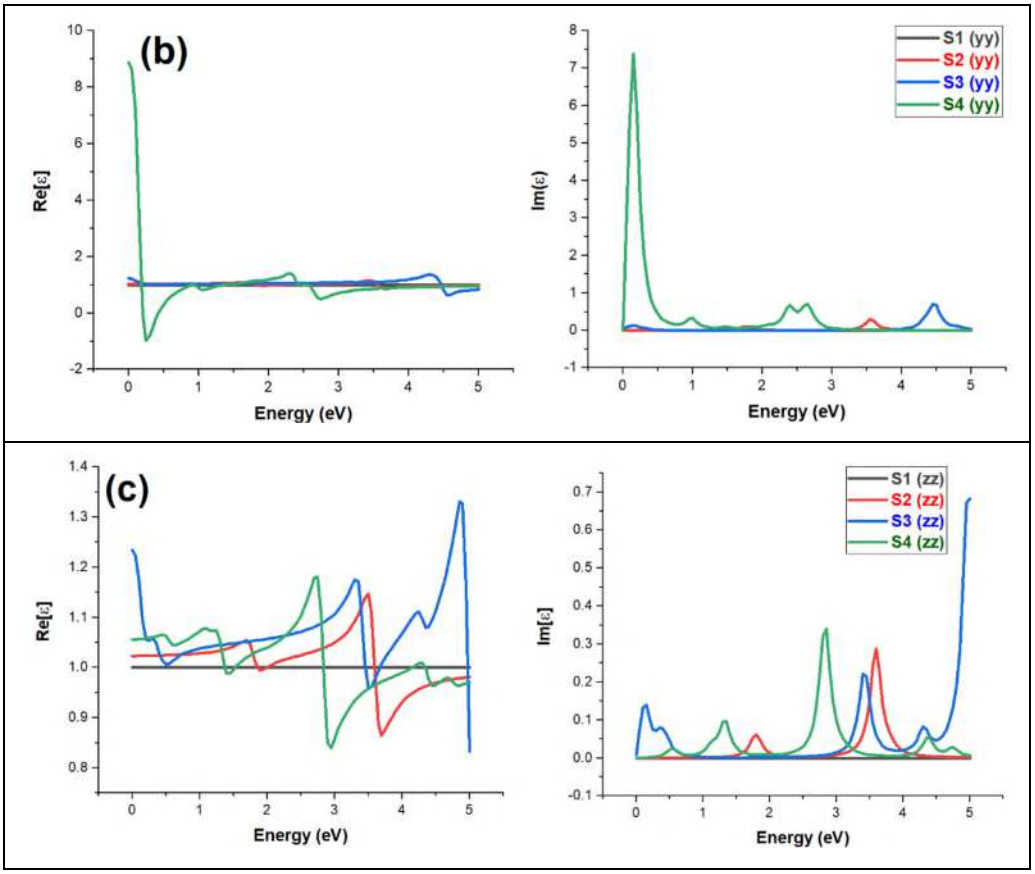

Fig.5 Dielectric constant of S1, S2, S3, and S4 along (a) xx, (b) yy, and (c) zz direction

Extinction (k) and Refractive Index (η)

The sum of scattering and absorption representing the total effect of medium on radiation passing the material is determined using extinction spectrum [44]. Reflection of light ($R(\omega)$) gives the relation between the η and k as

$$R(\omega) = \frac{(\eta - 1)^2 + k^2}{(\eta + 1)^2 + k^2} \qquad (5)$$

Optical extinction and optical refraction index peaks were observed at 0eV and 1eV for S1 shown in Fig.6 &7. Similarly, maximum optical extinction and optical refraction peaks of 0.5 and 1.2, 0.35 and 1.175, and 1.7 and 3 were observed at 1.9eV, 4.5eV, and 0.2eV for S2-S4 as shown in Fig.6 & 7. Identical maximum peaks were observed for optical extinction and refractive index for S2-S4. Thus, extinction and refractive plots validate the dielectric function $\varepsilon(\omega)$ of LD-SWBNNT material [46, 47].

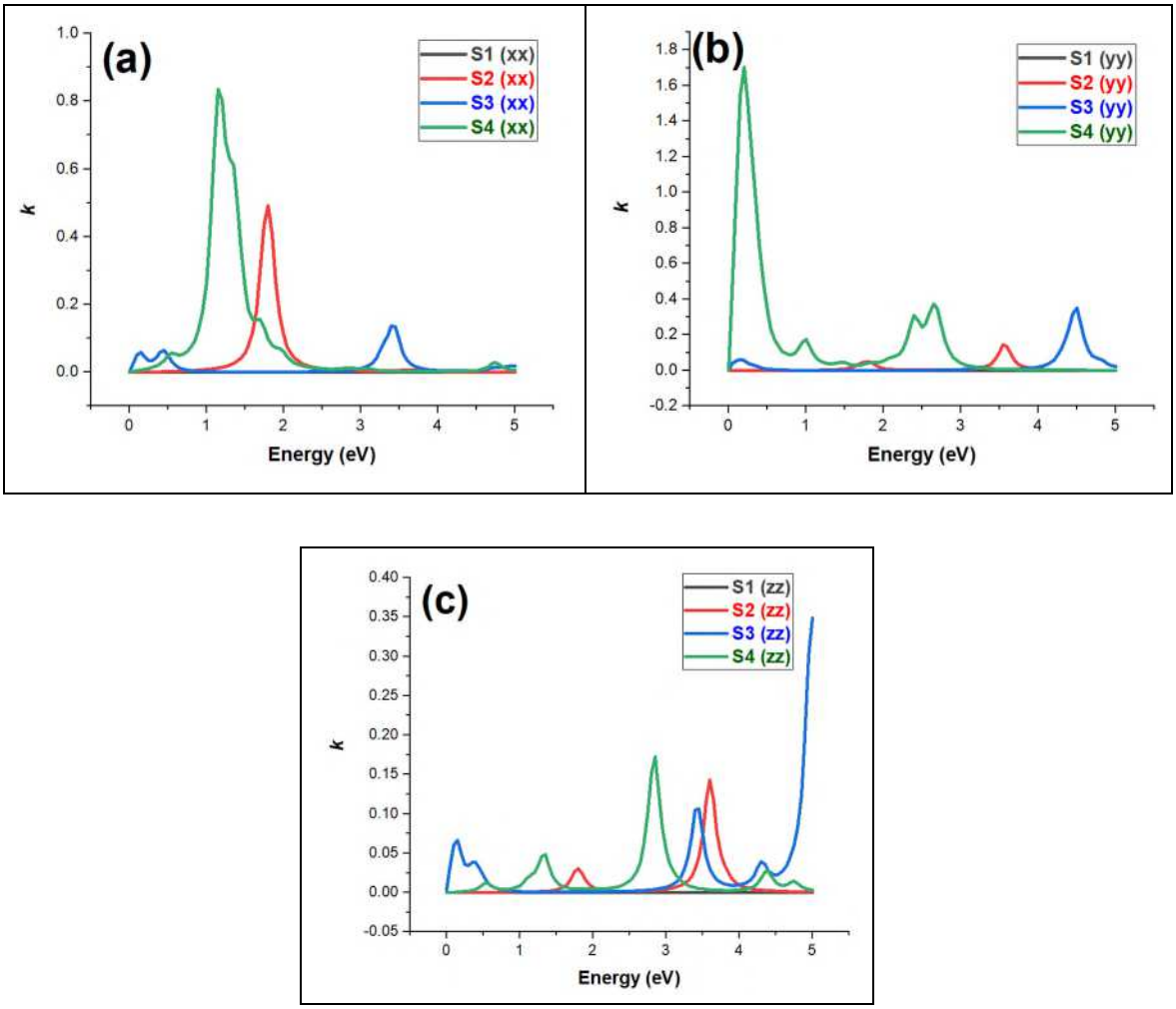

Fig.6 Extinction of S1, S2, S3, and S4 along (a) xx, (b) yy, and (c) zz direction

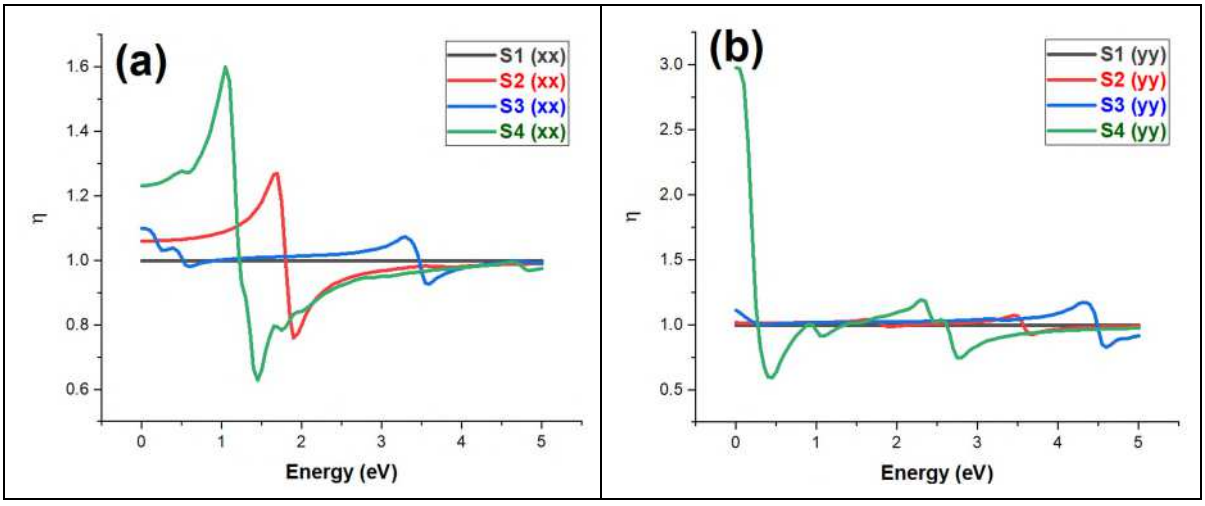

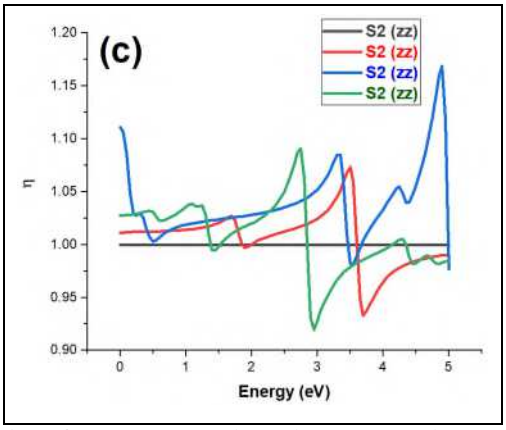

Fig.7 Refractive Index of S1, S2, S3, and S4 along (a) xx, (b) yy, and (c) zz direction

Optical conductivity (σ)

Optical conductivity also helps in determining the electrical conductivity of the low-dimensional materials [48, 49]. High optical conductivity of 2.22E-3, 2.5E-3, and 4E-3 Ω.cm was observed for S2-S4 along xx direction as shown in Fig.8(a). The lowest optical conductivity of 1.5e-09 $\Omega^{-1}cm^{-1}$ was observed for S1 shown in Fig.8, depicting its high resistivity along xx direction. S2, S3, and S4 samples can be used as composites in photoconductive devices [22].

High σ peaks were observed at 0.2eV (LRE), 1.8eV (LRE), 4.5eV (HRE) and 1.2eV (LRE) for S1, S2, S3, and S4, respectively. The maximum peak was observed in S1-S4 referring to low to high inter-band transition. High optical conductivity is due to the corresponding valence and conduction sub-bands transition (C_1-V_1, C_2-V_2) arises from the symmetry of Fe doped SWBNNT [47]. The study suggested that the energy of maximum optical conductivity increases with a decrease in diameter [50].

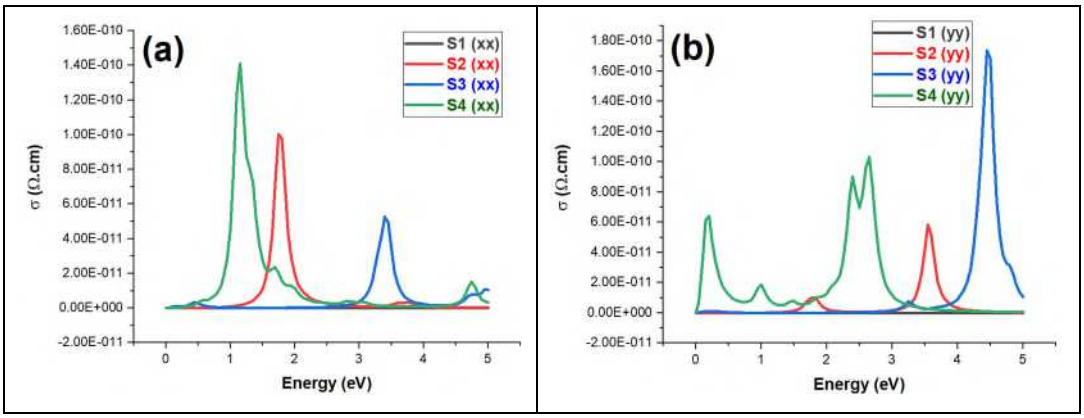

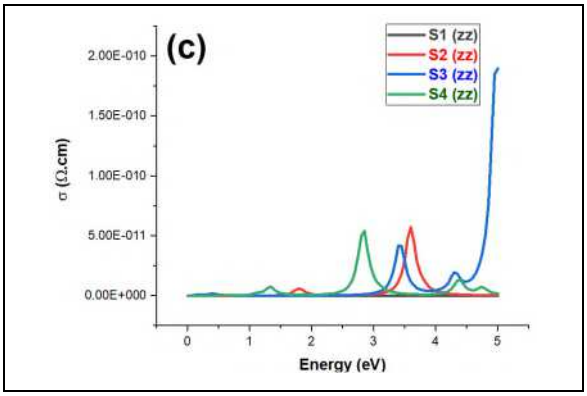

Fig.8 Optical conductivity of S1, S2, S3, and S4 along (a) xx, (b) yy, and (c) zz direction

Reflectivity (r)

The highest reflectivity of 0.35 is observed for S4 along yy direction as shown in Fig.9(b). The lowest reflectivity of 0 with a Reflective Index (η) of 1 was observed for S1. The reflectance of nanotubes $R(\omega)$ is calculated having prior knowledge of its dielectric function $\varepsilon(\omega)$ [51] given as,

$$R(\omega)=\frac{\left[1-\sqrt{\varepsilon(\omega)^2}\right]}{\left[1+\sqrt{\varepsilon(\omega)^2}\right]} \qquad \text{(vi)}$$

Optical reflectivity is the method to identify the nature of materials by measuring the incident beam fraction (transmitted or reflected) of monochromatic light onto a material [51]. Optical reflectivity of 0, 0.05 at 1.8eV, 0.05 at 4.5eV and 0.35 at 0.2eV were observed for S1, S2, S3, and S4 along zz direction respectively, as shown in Fig.9(c). S4 predicts the maximum reflectivity peak lying in LRE, whereas for S2-S3 maximum reflectivity peak lying in HRE. It is observed that directions perpendicular to the tube axis (i.e., xx and yy direction) have higher optical reflectivity. S4 has the highest reflectivity of 0.35 at 0.2eV, which predicts its implementation as a photoelectric sensor [47].

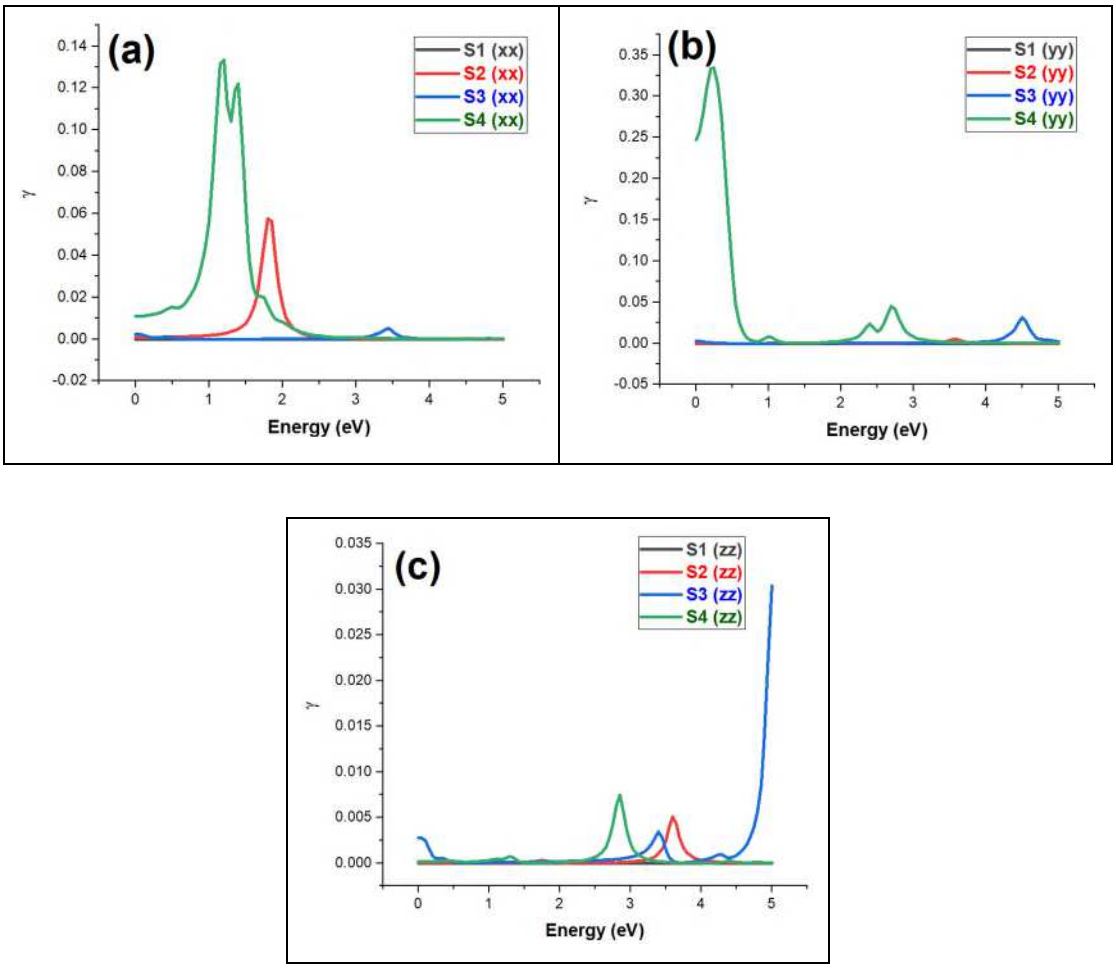

Fig.9 Reflectivity of S1, S2, S3, and S4 along (a) xx, (b) yy, and (c) zz direction

Susceptibility (χ)

The addition of Fe dopant in SWBNNTs has significantly increased the magnetic susceptivity in S2-S4 shown in Fig.10. S1 has a minimum χ of 6E-11, depicting its weak diamagnetic (χ <0) property. S2-S4 exhibited χ of 0.55, 0.4, and 7.6 respectively, depicting higher paramagnetic (χ >0) property. An increase in Fe dopant concentration leads to a rise in χ with stronger magnetic properties. Therefore,

predicts the possibilities of using LD Fe doped SWBNNT material as a ferromagnetic layer in nanodevices. Table VI shows the susceptibility (χ) at 0eV for S1, S2, S3, and S4 along xx, yy, and zz direction.

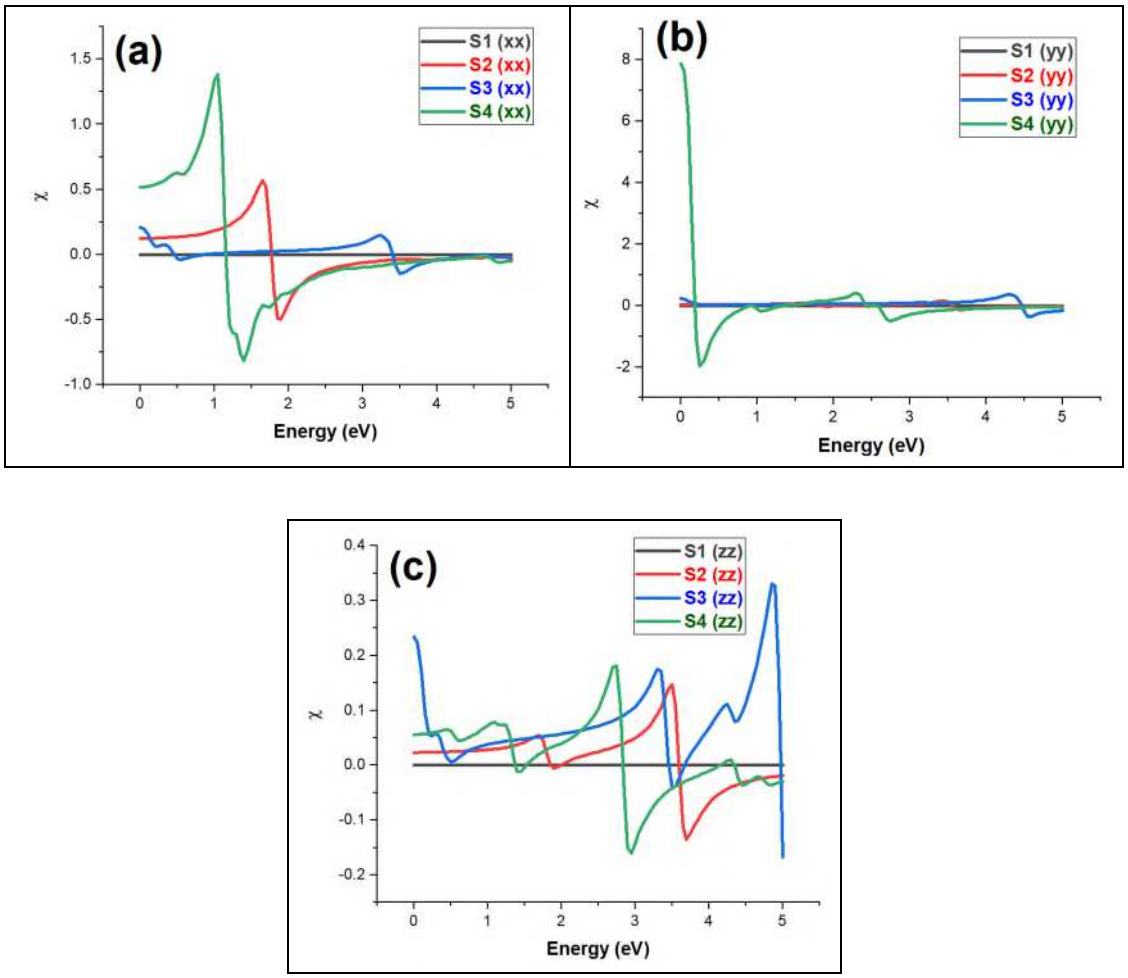

Fig.10 Susceptibility (χ) of S1, S2, S3, and S4 along (a) xx, (b) yy, and (c) zz direction

Table VI: Susceptibility (χ) at 0eV for S1, S2, S3, and S4 along xx, yy, and zz direction

Samples	S1 at 0eV	S2 at 0eV	S3 at 0eV	S4 at 0eV
χ along xx direction	5.55E-11	0.12	0.21	0.52
χ along yy direction	5.55E-11	0.04	0.24	7.87
χ along zz direction	-1.11E-16	0.02	0.23	0.06

IV. CONCLUSION

Atomistic computation based on EHTB methods was used for the analysis of SWBNNT with different Fe doping sites. Further, the electrical and optical parameters were determined using the Quantum ATK tool. The addition of Fe as a dopant in SWBNNT resulted in the increase of effective mass value for S2, S3, and S4 samples. The effective mass is an important parameter in the device perspective. The highest direct bandgap obtained for S1 and S3 was 5.3167eV and 3.5328eV at Γ point depicting its high-power electronic devices application. For S4 and S2, bandgap was obtained are 0.1448eV and 1.7113eV at Γ point with semiconductor characteristics. The SWBNNT shows a consistent bandgap with an increase in the length along the z-axis compared to CNT/SiCNT. The addition of Fe dopants leads to an increase in the number of peaks in DOS for SWBNNT, predicting its application in memory devices. A weaker and lesser number of DOS for S1 was observed in comparison to other samples.

From PDOS plots we observed N and Fe atoms as the majority contributor of electronic states in VB and Fe atom as the main contributor in CB.

Infirm optical excitation was observed due to lower SWBNNT density. The addition of Fe altered the absorption and wavelength properties (increase in Fe dopant leads to an increase in the wavelength and optical gap). The constant optical gap in S2 and S3 predicted applicability in nano-optoelectronic devices. From optical absorption vs wavelength plots of S2, S3, and S4 depicted its uses in the photodetector, LEDs, medical devices, and sensors. Dielectric constant (ε) is anisotropic for all the samples of SWBNNT. The imaginary part (ε_i) of ε peaks denote the direct interband transitions between the VHs as E_1 and E_2. Identical maximum peaks were observed for optical extinction and refractive index for S2-S4. High optical conductivity for S2-S4 were 2.22E-3, 2.5E-3, and 4E-3 Ω.cm along xx-direction, which can be used as composites in photoconductive devices. The lowest optical conductivity for S1 is 1.5E-09 $\Omega^{-1}cm^{-1}$ depicting its high resistivity along xx direction. The maximum energy of optical conductivity increased with a decrease in diameter. The highest reflectivity of 0.35 at 0.2eV is observed for S4 predicting its use in a photoelectric sensor such as smoke detectors. An increase in Fe dopant concentration led to a rise in χ . S1 has a minimum χ of 6E-11, depicting its weak diamagnetic (χ <0) property. S2-S4 present χ of 0.55, 0.4, and 7.6 respectively, showing higher paramagnetic (χ >0) property. BNNTs related technology is still in infancy, but the recent trend in BNNTs development has resulted in fascinating and promising applications in near future.

ACKNOWLEDGMENT

BS would like to thank All India Council for Technical Education (AICTE) Govt. of India for the support under Research Promotion Scheme for North-East Region (RPS-NER) vide ref.: File No. 8-139/RIFD/RPS-NER/Policy-1/2018-19.

REFERENCES

[1] Saikia N, Pati SK, Deka RC. First-principles calculation on the structure and electronic properties of BNNTs functionalized with isoniazid drug molecule. Applied Nanoscience. 2012 Sep;2(3):389-400.

[2] Kausar A, Rafique I, Muhammad B. Review of applications of polymer/carbon nanotubes and epoxy/CNT composites. Polymer-Plastics Technology and Engineering. 2016 Jul 23;55(11):1167-91.

[3] Blase X, Rubio A, Louie SG, Cohen ML. Stability and band gap constancy of boron nitride nanotubes. EPL (Europhysics Letters). 1994 Nov 10;28(5):335.

[4] Kim JH, Pham TV, Hwang JH, Kim CS, Kim MJ. Boron nitride nanotubes: synthesis and applications. Nano convergence. 2018 Dec;5(1):1-3.

[5] Golberg D, Bando Y, Kurashima K, Sato T. Synthesis and characterization of ropes made of BN multiwalled nanotubes. Scripta Materialia. 2001 May 18;44(8-9):1561-5.

[6] Bagheri Z, Mirzaei M, Hadipour NL, Abolhassani MR. Density functional theory study of boron nitride nanotubes: calculations of the N-14 and B-11 nuclear quadrupole resonance parameters. Journal of Computational and Theoretical Nanoscience. 2008 Apr 1;5(4):614-8.

[7] Chen X, Ke C. Structural and physical properties of boron nitride nanotubes and their applications in nanocomposites. InBoron Nitride Nanotubes in Nanomedicine 2016 Jan 1 (pp. 183-199). William Andrew Publishing.

[8] Zhi CY, Bando Y, Terao T, Tang CC, Kuwahara H, Golberg D. Chemically activated boron nitride nanotubes. Chemistry–An Asian Journal. 2009 Oct 5;4(10):1536-40.

[9] Zhi C, Bando Y, Terao T, Tang C, Kuwahara H, Golberg D. Towards thermoconductive, electrically insulating polymeric composites with boron nitride nanotubes as fillers. Advanced Functional Materials. 2009 Jun 23;19(12):1857-62.

[10] Zeng X, Sun J, Yao Y, Sun R, Xu JB, Wong CP. A combination of boron nitride nanotubes and cellulose nanofibers for the preparation of a nanocomposite with high thermal conductivity. ACS nano. 2017 May 23;11(5):5167-78.

[11] Kang JH, Sauti G, Park C, Yamakov VI, Wise KE, Lowther SE, Fay CC, Thibeault SA, Bryant RG. Multifunctional electroactive nanocomposites based on piezoelectric boron nitride nanotubes. Acs Nano. 2015 Dec 22;9(12):11942-50.

[12] Baierle RJ, Schmidt TM, Fazzio A. Adsorption of CO and NO molecules on carbon doped boron nitride nanotubes. Solid state communications. 2007 Apr 1;142(1-2):49-53.

[13] Wang R, Zhu R, Zhang D. Adsorption of formaldehyde molecule on the pristine and silicon-doped boron nitride nanotubes. Chemical Physics Letters. 2008 Dec 15;467(1-3):131-5.

[14] Wu X, Yang JL, Zeng XC. Adsorption of hydrogen molecules on the platinum-doped boron nitride nanotubes. The Journal of chemical physics. 2006 Jul 28;125(4):044704.

[15] Xiang HJ, Yang J, Hou JG, Zhu Q. Are fluorinated boron nitride nanotubes n-type semiconductors. Applied Physics Letters. 2005 Dec 12;87(24):243113.

[16] Li Y, Zhou Z, Zhao J. Functionalization of BN nanotubes with dichlorocarbenes. Nanotechnology. 2007 Nov 29;19(1):015202.

[17] Zhi C, Bando Y, Tang C, Golberg D. Engineering of electronic structure of boron-nitride nanotubes by covalent functionalization. Physical Review B. 2006 Oct 19;74(15):153413.

[18] Bernholc J, Brenner D, Buongiorno Nardelli M, Meunier V, Roland C. Mechanical and electrical properties of nanotubes. Annual Review of Materials Research. 2002 Aug;32(1):347-75.

[19] Wan X, Dong J, Xing DY. Optical properties of carbon nanotubes. Physical Review B. 1998 Sep 15;58(11):6756.

[20] Smidstrup S, Markussen T, Vancraeyveld P, Wellendorff J, Schneider J, Gunst T, Verstichel B, Stradi D, Khomyakov PA, Vej-Hansen UG, Lee ME. QuantumATK: an integrated platform of electronic and atomic-scale modelling tools. Journal of Physics: Condensed Matter. 2019 Oct 10;32(1):015901.

[21] Choudhary S, Goyal R. First-principles study of spin transport in CrO_2–graphene–CrO_2 magnetic tunnel junction. Journal of Superconductivity and Novel Magnetism. 2016 Jan 1;29(1):139-43.

[22] Gharbavi K, Badehian H. Optical properties of armchair (7,7) single walled carbon nanotubes. AIP Advances. 2015 Jul 23;5(7):077155.

[23] Rubio A, Corkill JL, Cohen ML. Theory of graphitic boron nitride nanotubes. Physical Review B. 1994 Feb 15;49(7):5081.

[24] Lee CH, Xie M, Kayastha V, Wang J, Yap YK. Patterned growth of boron nitride nanotubes by catalytic chemical vapor deposition. Chemistry of Materials. 2010 Mar 9;22(5):1782-7.

[25] Kayang KW, Nyankson E, Efavi JK, Abavare EK, Garu G, Onwona-Agyeman B, Yaya A. Single-Walled boron nitride nanotubes interaction with nickel, titanium, palladium, and gold metal atoms-A first-principles study. Results in Materials. 2019 Sep 1;2:100029.

[26] Lee CH, Bhandari S, Tiwari B, Yapici N, Zhang D, Yap YK. Boron nitride nanotubes: recent advances in their synthesis, functionalization, and applications. Molecules. 2016 Jul;21(7):922.

[27] Crespi VH, Cohen ML, Rubio A. In situ band gap engineering of carbon nanotubes. Physical review letters. 1997 Sep 15;79(11):2093.

[28] Dai H, Javey A, Pop E, Mann D, Kim W, Lu Y. Electrical transport properties and field effect transistors of carbon nanotubes. Nano. 2006 Jul;1(01):1-3.

[29] Misewich JA, Martel R, Avouris P, Tsang JC, Heinze S, Tersoff J. Electrically induced optical emission from a carbon nanotube FET. Science. 2003 May 2;300(5620):783-6.

[30] Valentini L, Armentano I, Kenny JM, Cantalini C, Lozzi L, Santucci S. Sensors for sub-ppm NO_2 gas detection based on carbon nanotube thin films. Applied Physics Letters. 2003 Feb 10;82(6):961-3.

[31] Delley B, Steigmeier EF. Quantum confinement in Si nanocrystals. Physical Review B. 1993 Jan 15;47(3):1397.

[32] Seo TH, Lee GH, Park AH, Cho H, Kim JH, Chandramohan S, Jeon SR, Jang SG, Kim MJ, Suh EK. Boron nitride nanotubes as a heat sinking and stress-relaxation layer for high performance light-emitting diodes. Nanoscale. 2017;9(42):16223-31.

[33] Wu X, Zeng XC. Adsorption of transition-metal atoms on boron nitride nanotube: A density-functional study. The Journal of chemical physics. 2006 Jul 28;125(4):044711.

[34] Wang W, Bando Y, Zhi C, Fu W, Wang E, Golberg D. Aqueous noncovalent functionalization and controlled near-surface carbon doping of multiwalled boron nitride nanotubes. Journal of the American Chemical Society. 2008 Jul 2;130(26):8144-5.

[35] Silva LA, Guerini SC, Lemos V. Electronic and structural properties of oxygen-doped BN nanotubes. IEEE transactions on nanotechnology. 2006 Sep 11;5(5):517-22.

[36] Sharma S, Rani P, Verma AS, Jindal VK. Structural and electronic properties of sulphur-doped boron nitride nanotubes. Solid state communications. 2012 May 1;152(9):802-5.

[37] Mirzaei M et al., A computational study of oxygen-termination of a (6,0) boron nitride nanotube. Monatshefte für Chemie-Chemical Monthly. 2010 May;141(5):491-4.

[38] Xu B, Ouyang J, Xu Y, Wu MS, Liu G, Ouyang CY. The structural, mechanical and electronic properties of (4, 4) SiC/C nanotube heterojunction: A first-principles study. Computational materials science. 2013 Feb 1;68:367-70.

[39] S.Q. Wang and H.Q. Ye, First-principles study on elastic properties and phase stability of III–V compounds, physica status solidi (b) 240(1), 45-54 (2003).

[40] C. Aurisicchio et al., Optoelectronic Devices: CNTs in Optoelectronic Devices: New Structural and Photophysical Insights on Porphyrin-DWCNTs Hybrid Materials, Advanced Functional Materials 22, 3209-3222 (2012).

[41] A. Martinez and S. Yamashita, in Carbon Nanotube-Based Photonic Devices, edited by J.M. Marulanda (The University of Tokyo, Japan: Tokyo, 2001).

[42] Ju SP, Wang YC, Lien TW. Tuning the electronic properties of boron nitride nanotube by mechanical uniaxial deformation: a DFT study. Nanoscale research letters. 2011 Dec;6(1):1-1.

[43] Dresselhaus MS, Dai H. Carbon nanotubes: continued innovations and challenges. MRS bulletin. 2004 Apr;29(4):237-43.

[44] Ambrosch-Draxl C, Sofo JO. Linear optical properties of solids within the full-potential linearized augmented planewave method. Computer physics communications. 2006 Jul 1;175(1):1-4.

[45] Haug H, Koch SW. Quantum theory of the optical and electronic properties of semiconductors. World Scientific Publishing Company; 2009 Jan 22.

[46] O'connell MJ, Bachilo SM, Huffman CB, Moore VC, Strano MS, Haroz EH, Rialon KL, Boul PJ, Noon WH, Kittrell C, Ma J. Band gap fluorescence from individual single-walled carbon nanotubes. Science. 2002 Jul 26;297(5581):593-6.

[47] Movlarooy T et al., The effect of intraband transitions on the optical spectra of metallic carbon nanotubes. Chinese Physics Letters. 2013 Jul;30(7):077301.

[48] Milošević I, Vuković T, Dmitrović S, Damnjanović M. Electro-optical properties of single-walled carbon nanotubes. Physica E: Low-dimensional Systems and Nanostructures. 2002 Jan 1;12(1-4):745-8.

[49] Damnjanovic M, Milosevic I, Vukovic T, Sredanovic R. Full Symmetry of Single-and Multi-wall Nanotubes. arXiv preprint cond-mat/9902245. 1999 Feb 17.

[50]] Movlarooy T, Kompany A, Hosseini SM, Shahtahmasebi N. Optical absorption and electron energy loss spectra of single-walled carbon nanotubes. Computational Materials Science. 2010 Sep 1;49(3):450-6.

[51] Kittel C, McEuen P, McEuen P. Introduction to solid state physics. New York: Wiley; 1996 Dec.

Declarations

Funding: The work is supported by All India Council for Technical Education (AICTE) Govt. of India under Research Promotion Scheme for North-East Region (RPS-NER) vide ref.: File No. 8-139/RIFD/RPS-NER/Policy-1/2018-19.

Conflicts of interest/Competing interests: The is no Conflict of Interest pertaining to the work submitted in this manuscript.

Availability of data and material: As such there is no hidden data. But, if required ca submit the available data required for carrying out this work.

Code availability: The is no separate coding carried out. It is a purely a computational work carried out via GUI on Quantum ATK software.

Authors' contributions: All authors have contributed to the formulation, design, computation, analysis and drafting of the manuscript respectively.

Ethics approval: NA

Consent to participate: NA

Consent for publication: Yes, all the authors consent for publication.